Computers and Electronics in Agriculture 114 (2015) 163–177

Contents lists available at ScienceDirect

Computers and Electronics in Agriculture

journal homepage: www.elsevier.com/locate/compag

Automated 3D reconstruction of grape cluster architecture from sensor data for efficient phenotyping

Florian Schöler, Volker Steinhage *

University of Bonn, Institute of Computer Science III, Römerstraße 164, 53117 Bonn, Germany

ARTICLE INFO

Article history:
Received 1 October 2014
Received in revised form 29 March 2015
Accepted 1 April 2015
Available online 21 April 2015

Keywords:
Phenotyping bottleneck
Non-invasive phenotyping
Phenotyping descriptors
Grapevine breeding

ABSTRACT

We propose an approach to fully-automated and sensor-based 3D reconstruction of grape cluster architecture followed by a precise, objective, and reproducible derivation of phenotypic traits. Current approaches to sensor-based phenotyping often show interactive processing steps and analyze only those parts of a plant that can be sensed by the given sensor system. Our approach employs an explicit component-based model of the architecture of grape clusters, i.e., the interconnectivity of a grape cluster's components, the geometry of the components, and the structural and geometrical constraints of their mutual connections. Based on this model, our approach can derive in a fully automated way complete 3D reconstructions of sensed grape clusters even for cases of partial occlusions in the process of sensor data acquisition. Given a complete 3D reconstruction of a grape cluster, we can derive on the one hand well known phenotypic traits of grape clusters. On the other hand, this approach facilitates measuring and evaluating new phenotypic traits. Therefore, our approach is of interest for monitoring and yield estimations in vineyards as well as for grapevine breeders. We developed and implemented our approach within a grapevine phenotyping project. First evaluations of reconstruction results and derived phenotypic traits show a potential of this approach for automated high-throughput phenotyping. We discuss the opportunities to apply our approach to other plants and with other sensor systems.

1. Introduction

1.1. Motivation

Phenotyping addresses two major objectives in plant breeding. First, phenotyping is used for the early identification of traits determining yield potential, stress resistance, and crop quality. Second, phenotyping is used to ascertain phenotype from interactions between genotype and environment. But phenotyping is widely recognized as being labor-intensive and of costly nature resulting in the so-called 'phenotyping bottleneck' (Furbank and Tester, 2011) in crop breeding. The phenotyping bottleneck can now be addressed by employing innovative technologies such as non-invasive sensor technology, robotics and high-throughput computing.

Within an interdisciplinary research network CROP.SENSe.net of *Bonn University, Germany,* and the *research centre Jülich, Germany,* several subprojects worked together on non-invasive and quantitative screening of plant phenotype throughout plants' lifecycles (CROP.SENSe.net, 2015). The different subprojects worked on different target plants. The target plant of subproject D2 – on which we report here – was grapevine (*Vitis vinifera* l. subsp. vinifera) and plant samples were provided by subproject partners of the *Julius-Kühn Institute for Grapevine Breeding* (JKI, 2015).

For comparing different grapevine cultivars there are mainly three institutes that work on a set of common descriptors for grapevine in its different growth stages and for different plant organs. These are: (1) *Organisation Internationale de la Vigne et du Vin* (OIV, 2015), (2) *International Union for the Protection of New Varieties of Plants* (UPOV, 2015), (3) *International Plant Genetic Resources Institute* (IPGRI, 2015), recently renamed to *Bioversity International.* OIV released their own catalogue of descriptors (OIV, 2009), but there is also a joint release of all three institutes (IPGRI et al., 1997). Development stages of grapevine are classified and categorized by the BBCH (Biological Institute of Agriculture and Forestry, Federal Organisation for Plant Varieties, and Chemical Industry (Lorenz et al., 1995). The OIV descriptor list (OIV, 2009) summarizes all established phenotypic traits of grapevine plants in general and grape clusters in particular, such as length, width and density of grape clusters (OIV descriptors 202, 203, and 204, respectively), the uniformity of berry sizes (OIV descriptor 222), and the average length of pedicels (OIV descriptor 238). In grapevine breeding, especially low density of grape

* Corresponding author. Tel.: +49 (0)228 734538.
E-mail address: steinhage@cs.uni-bonn.de (V. Steinhage).

http://dx.doi.org/10.1016/j.compag.2015.04.001
0168-1699/

clusters (OIV descriptor 204) is an important breeding objective with respect to better yield quality and higher disease resistance, especially to *Botrytis cinerea* (Vail and Marois, 1991).

Therefore, the objective of this subproject was the development of a sensor-based method for the automated 3D reconstruction of grape cluster architecture followed by a precise, objective, and reproducible derivation of phenotypic traits of grape clusters with special interest on the density descriptor. Additionally, the developed approach to automated 3D reconstruction and phenotyping of grape clusters should be applicable to different growth stages of the vine plant.

1.2. Approaches to 3D reconstruction of plants

In the context of biology, agronomy and phenotyping, acquisition of accurate models of real plants is still a difficult, cumbersome and expensive task and therefore a major bottleneck for the construction of quantitative models of plant development. Recently, 3D laser scanning has become a powerful and common approach to 3D measurements with high accuracy, spatial resolution and speed on nearly every scale range. These 3D measurements result in a multitude of 3D points – a so-called point cloud – representing a sampling of the surfaces of the scanned objects that require processing and analysis.

A variety of specific methods has been proposed to reconstruct plausible branching plant architecture from laser data, especially of trees (Raumonen et al., 2013; Livny et al., 2010; Preuksakarn et al., 2010; Côté et al., 2009; Runions et al., 2007; Xu et al., 2007). Mostly, these methods work in a *bottom–up strategy*, i.e., points are first grouped into larger components using methods of point set topology, graph theory, principal component analysis, optimization, etc. These more comprehensive components are then arranged and re-arranged using heuristic repair functions or optimization. All these steps are controlled by some specific heuristic parameters that are – at least partially – difficult to interpret since their semantics are defined as a mixture of domain specific knowledge of plant geometry and topology (i.e., shape, orientation, and connectivity parameters of plant components) on the one hand but also from pure technical necessities given by the mathematical concepts of the employed bottom–up segmentation methods on the other hand.

In contrast to these bottom–up plant reconstruction methods, top–down oriented approaches employ explicit generative plant models to guide the reconstruction process. For example, Huang and Mayer (2007) reconstruct 3D models of tree branch structure from image data using a generative model that describes the architecture of trees by an L-system (Prusinkiewicz and Lindenmayer, 1990). A Lindenmayer-, or in short L-system, is a parallel string rewriting system where a set of rules is used to generate structures of plants. Their reconstruction process employs a stochastic sampling to generate reconstruction hypotheses. They use Markov chain Monte Carlo sampling (MCMC). Given triplets or quadruples of images from single unfoliaged trees, they extract the trunk and the first two levels of the main branching system by multi-view image analysis and the generation of branches is controlled by the L-system. MCMC is used to propose size and orientation parameters of each new branch. That way several reconstruction hypotheses are generated using the L-system and MCMC sampling. The generated hypotheses are back-projected into the input images, to select the best fitting hypothesis as the final reconstruction result. Binney and Sukhatme (2009) employ also a generative approach. But while Huang and Mayer (2007) model branches by single straight cylinders, Binney and Sukhatme (2009) model branches as chains of fixed-length cylindrical segments. Therefore, they can represent and reconstruct curved branches. Their approach is working with laser range data measured from unfoliaged trees. The model-based approach of Shlyakhter et al. (2001) also employs an L-system but uses images of foliaged trees. Due to the large amounts of occlusions given in foliaged trees, their objective is not to reconstruct the exact architecture of the given tree, but a plausible approximation for visualization purposes. To do so, they reconstruct the visible trunk of the tree as well as the visual hull of the crown by means of multi-view image analysis. The trunk is used as the axiom of an L-system. The rewriting rules of the L-system are used to let the tree "grow" into the visual hull of the crown. Thereby, the rules of the L-system assure that no branch will grow out of the visual hull of the crown and simulate the flow of photosynthates inside the tree's branching structure to achieve a plausible distribution of leaves. It is worth noting that both approaches working on unfoliaged trees can validate branching points and branches using the likelihood of these part hypotheses with respect to the sensor data. Therefore, their optimization method can focus on parameter optimization of just these components. In contrast, the approach of Shlyakhter et al. (2001) to the reconstruction of foliaged trees has to deal with significant amounts of occlusions. Therefore, they cannot use evidence from sensor data to reconstruct the hidden interior branching structure. In consequence, they aim not to reconstruct the exact complete architecture of a scanned tree but just a plausible one. Thereby, they avoid to include the process of model selection, i.e., to optimize reconstruction results not only with respect to best fitting parameters of a generated model but also with respect to the selection of the best fitting number and classes of model components.

Additionally, there are various approaches to extract phenotypic traits of plant organs involving notations of plant models. But these approaches focus on certain plant organs of interest like leaves and stems (e.g., Dornbusch et al., 2007), need manual interactions (e.g., Buck-Sorlin et al., 2008; Frasson and Krajewski, 2007) or show no explicit modeling of interconnectivity (e.g. Paproki et al., 2012; Hartmann et al., 2011).

With respect to grapevine – as Furbank and Tester (2011) (Furbank and Tester, 2011), stated in their review on phenotyping in general: "the bottleneck in field phenotyping has driven intense interest over the past decade in applying remote sensing technologies to field crop monitoring and in this regard field phenomics is more advanced in many respects than controlled-environment, high-throughput analysis" – we can find several approaches to mapping and characterization of vineyard canopy by aerial multispectral imagery and satellite multispectral imagery (Delenne et al., 2010; Zarco-Tejada et al., 2005; Hall et al., 2003; Johnson et al., 2003). However, the availability of remotely sensed data is constrained by weather conditions, re-visit frequency and elaborate data processing. Emerging ground sensing technologies are attractive to get around the problem of availability and promise to deliver data of high spatial resolution to facilitate real-time applications. Therefore, several new studies of employing ground sensing technologies for an improved management of vineyards in practical viticulture have been conducted in recent years (Fuentes et al., 2014; Mazzetto et al., 2011; Llorens et al., 2011; Longo et al., 2010; Braun et al., 2010; Berenstein et al., 2010; Möller et al., 2007). Yield estimation is one of the most important issues in precision viticulture and several studies aimed to improve yield estimation by detecting grape clusters, berries (Kicherer et al., 2015; Roscher et al., 2014; Nuske et al., 2014; Font et al., 2014; Liu et al., 2013; Diago et al., 2012) or inflorescences (Diago et al., 2014) in images. Due to the importance of the density of grape clusters (OIV descriptor 204) with respect to grape and wine quality, there are also new studies aiming for an automated estimation of the density of grape clusters by evaluating indexes for density estimation (Tello and Ibánez, 2014) and applying image analysis to terrestrial field imagery or lab imagery to automate density estimation. This estimation can be done by measuring the proportion of pixels

in a bunch corresponding to berries, rachis, and holes (Cubero et al., 2015) or the difference between the convex hull of a cluster and its berries derived by a stereo approach (Ivorra et al., 2015).

While all of these studies show impressive results in detecting berries, grape clusters, or inflorescences to derive accurate models of grapevine for estimating yield, health status and quality of grapes and wine, all these studies focus mainly on vineyard management. In contrast, grapevine breeding aims at the phenotyping of single grapevines, where plants of different genotypes showing distinct phenotypes need to be assessed individually with high precision.

Therefore, we advocate enhancing the current quality of grapevine models by modeling and reconstructing their explicit, complete and detailed 3D architecture to derive from such reconstructions a rich set of phenotypic descriptors with high precision. The precise reconstruction of the complete 3D architecture can be done by employing sensor-based reconstruction approaches using generative models as shown within the approaches to 3D tree reconstruction already sketched in this section (Huang and Mayer, 2007; Binney and Sukhatme, 2009; Shlyakhter et al., 2001). With respect to grapevine, such an approach is reported by Huang et al. (2013). They describe a rule-based approach to the modeling of grape clusters using an L-system with the objective to create realistic renderings of several types of grape clusters. However, their approach relies heavily on user interaction to control the overall shape of the grape cluster and to determine parameter values. Therefore, it is not an approach to fully automated and sensor-based 3D reconstruction and automated phenotyping of grape clusters at all. Pallas et al. (2009) propose a stochastic growth model of grapevine that models interaction between environment, trophic competition and plant development. Thereby, this functional–structural growth model is focusing on the pure topology of grapevine and less on geometry. Therefore, 3D reconstruction and phenotyping is again not the objective of their work.

In conclusion, one can see that research on the sensor-based generation of accurate plant models and plant architecture in general shows considerable progress. Incomplete sensor data due to occlusions or just partial measurement of a plant as well as interleaving and closely neighbored plant organs and branches give rise to employ generative plant models. Explicit generative plant models also allow for meaningful parameterizations and user interfaces of automated approaches to plant reconstruction. For phenotyping of grapevine, there exists – to the best of our knowledge – no approach to sensor-based generation of detailed and accurate structural models of plants and plant organs. Additionally, there is no model-based approach to the reconstruction of plants that combines model selection (i.e., optimizing the number and interconnectivity of plant components) with parameter optimization (i.e., adjustment of geometrical and topological parameters of the plant components and their interconnectivity) to handle significant occlusions and interleaving branches.

From the methodological point of view, our work is most similar to the approaches described by Huang et al. (2013), Binney and Sukhatme (2009), Huang and Mayer (2007) and Shlyakhter et al. (2001). Their approaches also employ generative models to control the reconstruction process. However, Binney and Sukhatme (2009) and Huang and Mayer (2007) work on unfoliaged trees. Therefore, they can assume that they are able to detect and reconstruct the correct number of plant components, i.e., the correct number of relevant branches. Therefore, their optimization focuses on parameter adjustment and need not deal with the automated determination of the number of components, i.e., the so-called model selection. Unlike these approaches, our optimization problem is a trans-dimensional optimization problem, i.e., we have to determine automatically the number of components of a grape cluster and we have to optimize the parameterization of these components. In principle, Shlyakhter et al. (2001) also have to solve a trans-dimensional optimization problem since they work on foliaged trees with significant amounts of occlusions. But they avoid its explicit solution, because they are only interested in the reconstruction of "a plausible branching structure [that] suffices to preserve the overall impression of the original" (Shlyakhter et al., 2001: p. 53) while we are aiming for the exact structural reconstruction of a grape cluster to facilitate phenotyping. Finally, Huang et al. (2013) work exactly on the same topic as we do, but they aim for realistic renderings of several types of grape clusters instead of precise reconstruction and phenotyping. Therefore, they allow multiple user interactions to control the overall shape of the grape cluster and to determine parameter values, whereas we are aiming for a fully automated approach that is potentially suited for high throughput phenotyping. Additionally, they do not have to solve the optimization problem due to interactive parameter selection by the user.

1.3. Contributions and overview

The contribution of this study is the conceptual design, implementation, and evaluation of a complete processing chain that uses 3D point clouds of grape clusters produced by a laser range sensor and that employs an explicit generative model of grape cluster architecture to enable a fully automated 3D reconstruction and phenotyping of grape clusters sensed by laser scanning. The reconstruction procedure thereby combines model selection (i.e., optimizing the number and interconnectivity of plant components) with parameter optimization (i.e., adjustment of geometrical and topological parameters of the components of grape clusters and their interconnectivity). The results of the reconstruction procedure are complete, detailed and accurate structural models of the sensed grape cluster architectures allowing the derivation of phenotypic traits in an automated, precise, and objective way.

The plant material and sensor are introduced in Sections 2.1 and 2.2. In Section 2.3 the proposed reconstruction and phenotyping framework and its processing steps is introduced. Section 2.4 describes the design and implementation of the generative model of grape cluster architectures. Section 2.5 explains the processing steps of the reconstruction and phenotyping framework in more detail. The experiments and the obtained results are presented in Section 3 and discussed in Section 4. Section 5 summarizes and concludes this study with avenues for future work.

2. Materials and methods

2.1. Plant material

We selected three development stages of grapevine grape clusters of the cultivar Riesling (*Vitis vinifera* L. 'Riesling'). According to the BBCH classification these have been:

- BBCH73: Berries are groat-sized. Berries are still growing; most of the stem system is visible.
- BBCH81: Berries are at the beginning of ripening. Berries have almost gained their maximum size and weight. Depending on the density of the specific cultivar's grape clusters, the interior – the stem system –is mostly occluded by the berries.
- BBCH89: Berries are ripe for harvest. Berries have gained their maximum size and weight. Depending on the density of the specific cultivar's grape clusters, the stem system can be completely occluded by the berries.

From these three development stages of grapevine, BBCH89 is the most challenging with respect to the objective of deriving a complete 3D reconstruction of a grape cluster's architecture. In this stage, especially the interior stem system of this architecture is highly occluded by the exterior fully developed berries. Even development stage BBCH81 shows significant occlusions of the interior stem system. In the ongoing argumentation, we refer mainly to our experiments with the most challenging development stages of grapevine, namely BBCH89. In the following discussion we will include the other two development stages BBCH73 and BBCH81. We had a total of 20 grape clusters available for each of the three stages. The grape clusters are between 9.5 cm and 13 cm long and between 5.8 cm and 8.5 cm wide.

2.2. Sensor

We used the Perceptron ScanWorks V5 (Perceptron Inc., 2015) attached to a Romer Infinite 2.0 articulated arm (Hexagon Metrology, 2015) as sensor. The sensor produces lines of 7640 point measurements at a frequency of 60 Hz with an accuracy of 0.024 mm. When moving the sensor around the object, consecutive line measurements are aggregated into a single coordinate frame by the software that comes with the sensor. The results are highly dense 3D point clouds. Fig. 1 depicts such a 3D point cloud generated from a grape cluster.

For our experiments we scanned the grape clusters twice. First, we generated laser scans of the complete grape clusters. Second, we scanned their stem systems, i.e., scans of the same grape clusters after having removed their berries.

2.3. Reconstruction and phenotyping framework

A four-step framework was developed in order to reconstruct a grapevine cluster and to estimate its phenotypic descriptors from point clouds derived by laser scanning of the grapevine cluster.

Step 1: *Automatic detection and reconstruction of berries and peduncle.* Given grape clusters of development stage BBCH89, the berries are ripe for harvest and cause maximum occlusion to the interior branching architecture of the grape cluster. Therefore, the berries will represent together with the peduncle the exterior and visible components of the grape cluster and are used as data-driven anchor points for the complete reconstruction.

Step 2: *First guess of the complete architecture of the grape cluster.* This initial reconstruction hypothesis need not be perfect! A less accurate initial hypothesis simply means that more intermediate hypotheses will be generated in the following optimization step in order to achieve a good result. Ideally, the initial guess is a model of a grape cluster that is sufficiently specific for being a good starting point for the following optimization process. Therefore, topology and geometry of such an initial guess model will be chosen from previous reconstruction results.

Step 3: *Optimization of the complete architecture.* The optimization process generates iteratively new reconstruction hypotheses of the complete grape cluster. In every step of this process a new hypothesis is generated by a local modification of the last hypothesis. Local modifications, so-called *jumps*, can change parameter values of given components of the grape cluster's reconstruction hypothesis but can also modify the number of the components by adding or removing berries, branches, twigs, etc. The acceptance of a new hypothesis depends on how well it complies with the sensor data in terms of likelihood.

Step 4: *Derivation of phenotypic descriptors.* Given the reconstruction of the complete architecture of a grape cluster, the derivation of phenotypic descriptors of grape cluster can be done in a precise, objective, and reproducible way. It is important to note that this can be done for well-known descriptors (e.g. from the OIV list of descriptors) as well as for newly formalized descriptors, which enables the design and evaluation of novel descriptors in grapevine breeding research.

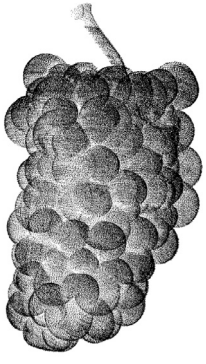

Fig. 1. Left: Sensor setup. A Perceptron *ScanWorks V5* is mounted onto a *Romer Infinite 2.0* articulated arm. Right: An example point cloud depicting a scanned grape cluster with 251,348 points.

All the steps of the reconstruction and phenotyping framework are guided by a generative model. The generative model describes by rules and parameter value distributions how every specific reconstruction result of an individual grape cluster is built up and how probable the parameter values (numbers of components, sizes of components, etc.) are. Therefore, the generative model first has to be specified based on expert knowledge and/or training data. Training data consist of a representative set of grape clusters and sensor data derived from these. Here, we used point clouds generated from grape clusters and their stem systems. The generation of the generative model comprises two aspects.

First, the generative model must provide entities to represent every grape cluster in its complete architecture with all its components. This includes the representation of every hypothesis that is generated in the steps of the reconstruction process, i.e., the reconstructed berries, the first guess, every intermediate and final reconstruction result. The rules of the generative model define elementary construction steps for building a grape cluster's architecture. This includes all jumps that are used in the optimization procedure. The rules define thereby also topological constraints on the architecture of possible instances of the generative model in specifying what kinds of components are allowed to be connected to what other kinds of components.

Second, the generative model must provide additional geometrical and numerical constraints on the components of grape clusters. Therefore, the rules are parameterized. Parameter values specify values of size (e.g., diameter of a berry, length and thickness of a branch, etc.), values of orientation (e.g., angles between branches, etc.), and values of quantities (e.g., number of berries per berry group, numbers of pedicels per pedicel origin, etc.). For every parameter a value distribution has to specify what values are how probable with respect to "real-world" experience given by an expert and/or by learning from training examples.

Fig. 2 summarizes all processing steps of the reconstruction and phenotyping framework. The bottom part of the figure depicts the

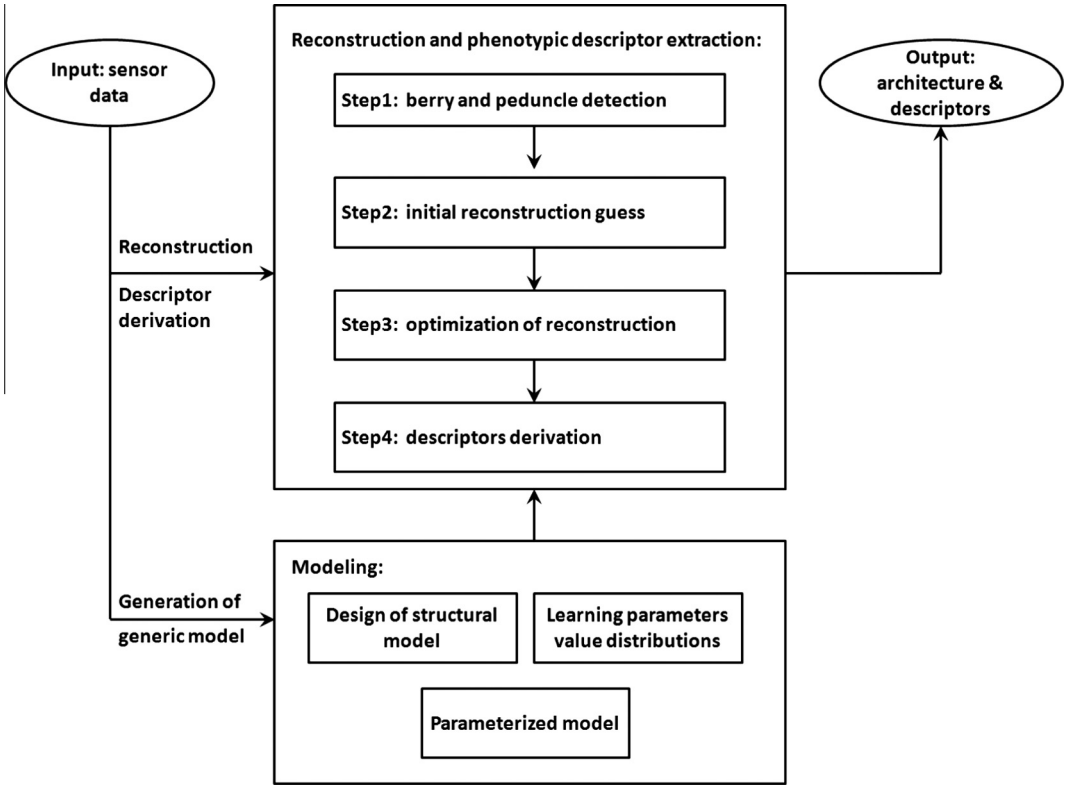

Fig. 2. Processing steps of the reconstruction and phenotyping framework. The bottom part shows the generation of the generative model based on training data. After having built the generative model, it is used to control the four steps of reconstruction and phenotyping of newly sensed grape clusters.

generation of the generative model that is based on a training data set of sensor data scanned from representative grape clusters. The first part of model generation is the design and implementation in terms of a rule-based system (cf. Section 2.4.1). The second part of model generation is the learning of value distributions of the parameters of the model (cf. Section 2.4.2). After having built the generative model, it is used to control the four steps of reconstruction and phenotyping of newly sensed grape clusters. These steps are depicted in the top part of the figure. Starting with the detection and reconstruction of the visible and therefore well sensed exterior components (for fully ripe grape clusters: exterior berries and peduncle) as step 1 (cf. Section 2.5.1), a first coarse reconstruction hypothesis is generated in step 2 (cf. Section 2.5.2). This initial hypothesis is iteratively optimized in step 3 (cf. Section 2.5.3). After optimization of the reconstruction hypothesis, phenotypic descriptors are derived in step 4 (cf. Section 2.5.4).

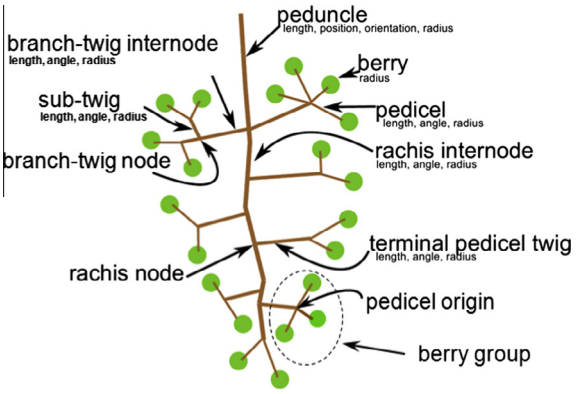

Fig. 3. Principal example of a grape cluster's architecture. Typically, a grape cluster has three different types of twigs (*branch-twig, sub-twig, terminal pedicel twig*), all of which are connected to the *rachis*. *Berries* are attached to the *twigs* and the *rachis* by *pedicels*.

2.4. Generative model

Fig. 3 depicts the components of a grape cluster, their parameters and their interconnectivity. The position and orientation parameters of the peduncle are specified with respect to a Cartesian coordinate system that is automatically established with the scanning process. Angles are specified with respect to their preceding component.

The central axis of a grape cluster consists of the *peduncle* on the top and the *rachis*, which holds different *twigs*, showing different types. A so-called *terminal pedicel twig* branches off the *rachis* and has further branches only at the end (hence: terminal) into the *pedicels*. So-*called branch-twigs* also branch off the *rachis* and differ from *terminal pedicel twigs*, because *branch-twigs* also bear further twigs, the so-called *sub-twigs*. All twig types and the *rachis* end in a set of *pedicels*. We call such a set of pedicels a *berry group* and they branch off the same *pedicel origin*. The *twigs* and the *rachis* are specified by the length and the radius of their *internodes* and by the angles of the *internodes* relative to the parent component.

It is important to note that this informal description specifies implicitly hard constraints on the possible interconnections in a grape cluster. These constraints become explicit in the formalization of the rules of the rule-based generative model and their parameters. For example, each *berry* is directly connected only to exactly one *pedicel*. In the reconstruction process it is disallowed to connect a berry directly with the rachis or any kind of twig.

2.4.1. Rule-based model of grape clusters

To formalize and implement the generative model and its constraints, we employ a relational growth grammar. The concept of

relational growth grammar (RGG) was introduced in Kniemeyer (2008), Kniemeyer et al. (2008) and Hemmerling et al. (2008). An RGG works similar to an L-system: A data structure representing a description of the state of a plant is iteratively modified by rewriting rules. For an RGG this data structure is a graph, consisting of nodes, which are also called modules, and edges. The modules represent plant components and the edges represent relations between them. Relations can be of different kind: physical connectivity, nutrition flow, relative shadowing effects, etc. In an RGG it is allowed to not only rewrite a single module, but also a subgraph or even a set of subgraphs within just one rewriting rule. Since the whole graph can be inspected, also the context of a rewriting rule can be a set of subgraphs. The RGG formalism was developed with the concepts of L-systems in mind. Therefore, while all important extensions of the L-system formalism are captured, relational growth grammars grant much more explicit modeling power. Simultaneously with the RGG concept the software GroIMP (Growth Grammar related Interactive Modeling Platform) was developed to implement RGGs. GroIMP comes along with features such as a compiler for the special purpose language XL and 3D rendering via OpenGL. It also provides a simple plug-in interface that allows users to write their own additions for GroIMP. For example, we added a plug-in for reading and processing of 3D point clouds for our experiments. GroIMP is constantly extended, for example, for specifying differential equations (Hemmerling et al., 2013).

2.4.2. Learning of parameter value distributions

Having formalized the generative model of a grape cluster's components and their relations, the value distributions of the model's parameters have to be determined. To derive the parameter value distributions of the branching architecture, we apply an automatic Skeletonization method (Balfer et al., 2013) to point clouds that were scanned from the stem systems of our training examples after berries from the grape clusters were removed (Schöler et al., 2013). Fig. 4 shows in the left part the point cloud of a scanned stem system and in the right part the derived skeleton. For each stem system we derive values for the components' lengths, angles, and frequencies. The statistics of these values are used to estimate the value distributions of the model's parameters. For the size parameters of the berry, we proceed analogously on the berries of our sensed grape clusters.

2.5. Reconstruction and phenotyping

2.5.1. Step 1: Detection of berries and peduncle

Besides the exterior berries, the peduncle of a grape cluster – even in the development stage of full ripeness – is always observable. Geometrically, we approximate the shape of a peduncle by a frustum (see Fig. 5). For the given grape clusters of the cultivar Riesling in our experiments, we can approximate the shape of berries by spheres (for other cultivars of grapevine, ellipsoidal shapes might be a more appropriate approximation). Therefore, we implement the detection of berries by a RANSAC-based detection of spheres in point clouds proposed by Schnabel et al. (2007). They also show that their approach to sphere detection in point clouds is applicable to the detection of other simple geometrical shape approximations like cones, cylinders, and frusta, and therefore can be directly extended to other types of berries.

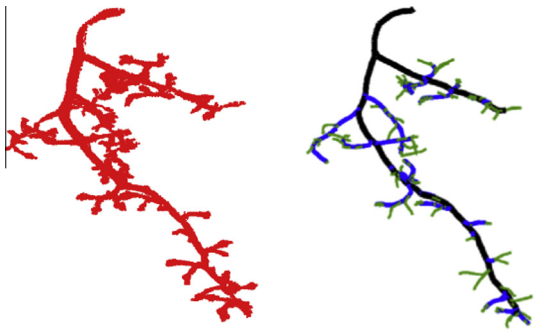

Fig. 4. An example of a point cloud of a stem system (left) and its computed skeleton (right) with semantic annotations for distinguishing between components. Here different semantic labels (rachis, branch twigs, terminal pedicel twigs) are depicted by different colors. (For interpretation of the references to color in this figure legend, the reader is referred to the web version of this article.)

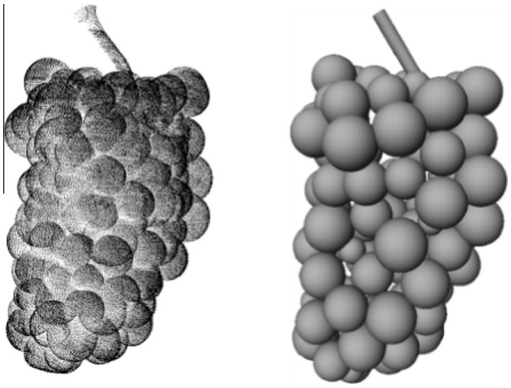

Fig. 5. Example of the reconstruction of the visible components, i.e., the berries and the peduncle, represented as spheres and a frustum, respectively.

2.5.2. Step 2: Initial guess of the complete reconstruction

The initial reconstruction guess is derived heuristically. First, the berries are grouped in berry groups, then the rachis is inserted, and finally the berry groups are connected to the rachis. Fig. 6 illustrates these three steps.

For the grouping of *berries*, we use k-means clustering (MacQueen, 1967) applied to the *berries*' centers, with a fixed $k = 20$. This heuristic parameter is the average number of berry groups that is estimated from our training data. The centers of these clusters define the initial positions of *pedicel origins* and are then connected to the corresponding *berries* by *pedicels*. In the next step, detailed in the following paragraph, the *rachis* is inserted, which is then used to connect the *pedicel origins* in the simplest way, i.e. directly via *terminal pedicel twigs*.

The insertion of the rachis is done in several steps. Fig. 7 illustrates this process. During the scanning process, the grape clusters were fixated in such a way that the peduncle forms the uppermost part of the grape cluster which itself is hanging downwards. To insert a first guess of the rachis, we divide the distance between the bottom end of the peduncle and the farthest pedicel origin into $r = 2$ equidistant planes. The heuristic parameter r is derived empirically by inspection of our training data set. For each plane we compute the intersections of that plane with the detected berries. These intersections result in a set of circles for each plane. The circles' centers are used to define the corner points of a convex polygon in every plane. Finally, the centers of these convex polygons are interpreted as rachis internodes. Between the peduncle, these internodes, and the farthest pedicel origin, frusta are inserted to form the complete initial guess of the rachis.

It must be stressed again: this heuristic approach to the construction of the initial reconstruction guess must not yield a very good or even perfect model. A less accurate initial model simply implies that in the following optimization process more local refinements will be applied to achieve the final optimal result.

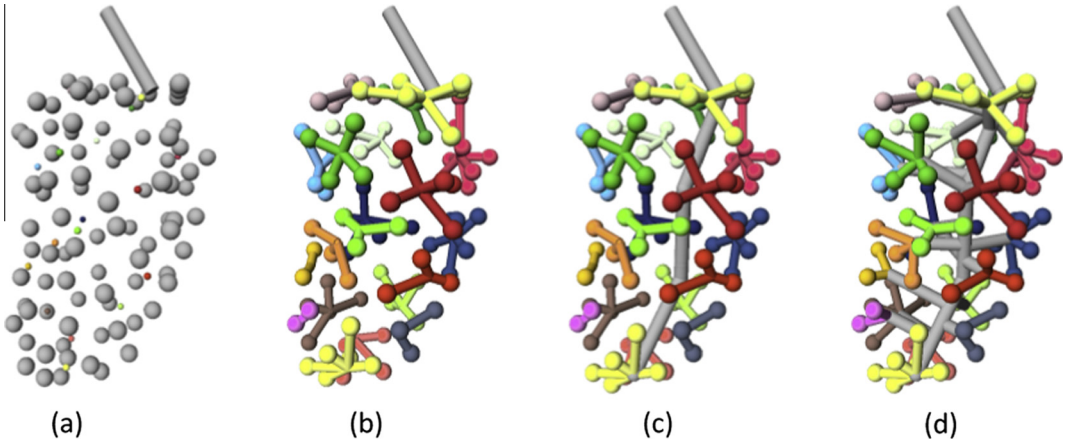

Fig. 6. Illustration of the reconstruction completion. Berries are reduced in size for the visualizations, while computations were done with the original sizes (a). After grouping of berries (b), the rachis is inserted (c). Finally, the berry groups are connected to the rachis via terminal pedicel twigs (d).

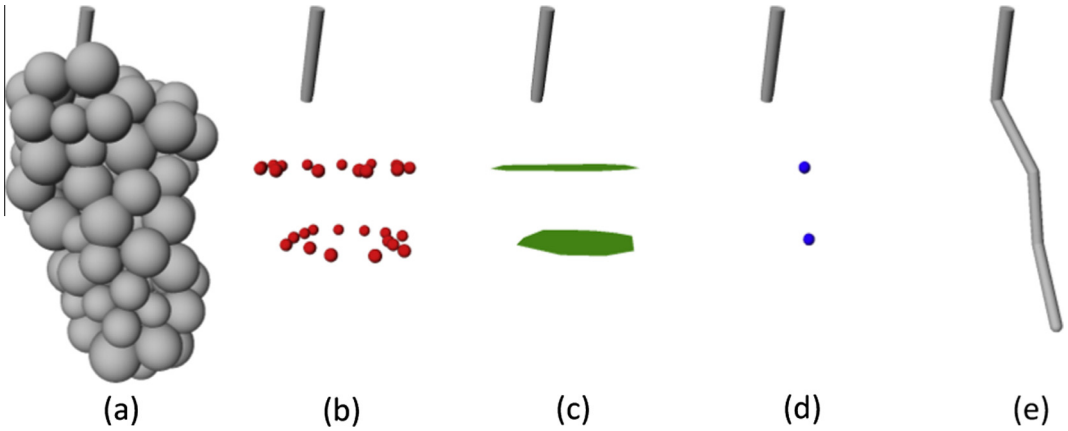

Fig. 7. Illustration for the insertion of a rachis into the detected berries. Based on the detected berries (a), for equidistant planes the intersections with the berries are computed (b). For each plane's intersections the convex polygon (c) is used to determine its center of mass (d). These centers are then used to insert the rachis internodes (e).

2.5.3. Step 3: Optimization of the complete reconstruction

The initial guess represents the first reconstruction hypothesis of the scanned grape cluster. Different hypotheses show different numbers of components and/or different parameterizations of their components. In general, the complete space of reconstruction hypotheses is infinite. Therefore, an exhaustive search for the hypothesis that fits the sensor data best is illusory.

Instead, we employ a probabilistic sampling approach that aims to terminate with the hypothesis that maximizes the likelihood with respect to the sensor data. To this end, we reformulate our reconstruction problem as a Bayesian decision problem with:

- $\boldsymbol{D}$, the set of sensor data: a laser point cloud, i.e., a finite subset of the 3-dimensional real-valued coordinate space $\mathbb{R}^3$,
- $\boldsymbol{S}$, the state space, i.e., the space of reconstruction hypotheses,
- x, an element of the state space representing a reconstruction hypothesis.

We consider a random variable X distributed in $\boldsymbol{S}$ where X follows a probability distribution that is the posterior distribution $p(x|\boldsymbol{D})$ of a reconstruction hypothesis x given sensor data $\boldsymbol{D}$. In a Bayesian framework, this posterior distribution function can be obtained from:

$$p(x|\boldsymbol{D}) \propto p(x) \cdot \mathcal{L}(\boldsymbol{D}|x).$$

The likelihood $\mathcal{L}(\boldsymbol{D}|x)$ represents the probability of observing sensor data $\boldsymbol{D}$, given reconstruction hypothesis x. The prior distribution $p(x)$ favors reconstruction hypotheses x that are compatible with the generative model. Based on this Bayesian formulation, the objective is to find the reconstruction hypothesis x that maximizes the posterior distribution function, i.e. the maximum a posteriori (MAP) estimator x_{MAP}. This is a non-convex optimization problem in a high-dimensional state space $\boldsymbol{S}$. Additionally, this optimization problem is a so-called *trans-dimensional optimization problem*, since the state space $\boldsymbol{S}$ shows varying dimensions as different reconstruction hypotheses show different numbers of components and therefore different numbers of parameters.

The Reversible Jump Markov Chain Monte Carlo (RJMCMC) algorithm (Green, 2003, 1995) is well adapted to such an optimization problem as RJMCMC allows the simulation of the posterior distribution on spaces of varying dimensions. Like standard Markov Chain Monte Carlo (MCMC) algorithms, RJMCMC simulates a random walk on the hypotheses, i.e., on the state space by iteratively proposing follow-up hypotheses and then accepting or rejecting these proposals as the new current step of the random walk. Each new step updates a series $(p^{(t)}(X^{(t)}))_{t\in\mathbb{N}}$ of probability distributions $p^{(t)}(X^{(t)})$ on the state space $\boldsymbol{S}$ with stationary distribution $\pi(X^{(t)})$ such that the stationary distribution $\pi(\cdot) = \not{p}(\cdot)$, where $\not{p}(\cdot)$ is the distribution of probabilities of the hypotheses with respect to the data $\boldsymbol{D}$. Therefore, samples are drawn only after having reached the stationary distribution and the maximum of

this stationary distribution is what must be found as the optimal reconstruction result.

In contrast to standard MCMC, RJMCMC allows to jump dimensions. This is accomplished by defining a set of state transitions, known as *jumps*. In this scheme, any state transition must be reversible, i.e. it must be possible to revert back to the previous state in a later move (Green, 1995: p. 713 ff.).

2.5.3.1. Jumps. In our framework for grape cluster reconstruction, the jumps are implemented by rewriting rules of the rule-based generative plant grammar. This means, there are rules that add or delete components (like twigs, pedicels, berries, etc.) to jump from one hypothesis to another. The selection and design of jump types is the crucial aspect in composing an RJMCMC sampler. There has to be a balance between jumps proposing large state changes for exploring the hypothesis space and jumps proposing small state changes for refining a given hypothesis. The jump types also have to cover all plant components. Finally, we want to have a minimal number of jump types preventing too many iterations of the sampler. We propose a set of jump types that shows on the one hand trans-dimensional jumps that add or delete components. For example, we can combine two terminal pedicel twigs into a single new one or we can add new berries in the occluded interior of the cluster. On the other hand, there are jumps for the refinement of a hypothesis by modifying size, position or orientation of some components. Fig. 8 shows two examples.

Our implementation of the RJMCMC sampler shows 14 different types of jumps that cover all components of a grape cluster. For example, the jump type *Combine terminal pedicel twigs* selects at random two terminal pedicel twigs and replaces these by a new single terminal pedicel twig that inherits all pedicels and berries of the two former terminal pedicel twigs. The random selection is constrained such that the given input twigs are sufficiently close to each other and have in total less than the maximum allowed number of attached berries per berry group. The reverse jump type is called *Split terminal pedicel twigs*.

2.5.3.2. Drawing samples. Now, RJMCMC implements the maximum a posteriori estimator x_{MAP} by iteratively proposing follow-up hypotheses and accepting or rejecting these proposals. Given $x^{(t)} = x$ at iteration t, RJMCMC shows three steps according to Green (1995):

(1) Choose a jump with proposal probability $q_j(x|.)$.
(2) According to $q_j(x|.)$, propose a new state x'.
(3) Accept $x^{(t+1)} = x'$ with probability

$$min\left(1, \frac{p(x' \mid \boldsymbol{D})}{p(x \mid \boldsymbol{D})} \cdot \frac{q_{j'}(xx')}{q_j(x'x)}\right)$$

and take $x^{(t+1)} = x$ otherwise.

According to Green (1995) the acceptance probability given as second argument of the minimization function in the acceptance step is generally a product of four fractions. But given a specific application, a careful design of the jumps and their distributions can reduce this to tractable expressions as explained in more detail by Schöler (2014) and Smith (2007). The decision of acceptance is based on a comparison with the current state x (i.e., the current reconstruction hypothesis). The transition $\mathcal{T}(x'|x)$ from state x to follow-up state x' shows two components: first, the application of a jump with a proposal probability $q(x'|x)$, i.e., how likely is this proposal of state x' given state x. Second, the probability of acceptance $\mathcal{A}(x'|x)$, i.e., how much better is the proposed state x' compared to the given state x. Therefore the transition probability becomes $\mathcal{T}(x'|x) = q(x'|x) \cdot \mathcal{A}(x'|x)$. Given the stationary distribution $\pi(\cdot) = p(\cdot)$, the detailed balance condition holds. The detailed balance condition states that for any pair of states x and x' the probability of being in x and transitioning to x' is the same as being in x' and transitioning to x, i.e., $p(x) \cdot \mathcal{T}(x'|x) = p(x') \cdot \mathcal{T}(x|x')$ for all x and x' of $\boldsymbol{S}$. The detailed balance condition can be rewritten as follows:

$$\begin{aligned} & p(x \mid \boldsymbol{D}) \cdot \mathcal{T}(x'|x) && = p(x' \mid \boldsymbol{D}) \cdot \mathcal{T}(x|x') \\ \Longleftrightarrow\ & p(x \mid \boldsymbol{D}) \cdot q(x'|x) \cdot \mathcal{A}(x'|x) && = p(x' \mid \boldsymbol{D}) \cdot q(x|x') \cdot \mathcal{A}(x|x') \\ \Longleftrightarrow\ & \frac{\mathcal{A}(x'|x)}{\mathcal{A}(x|x')} && = \frac{p(x' \mid \boldsymbol{D}) \cdot q(x|x')}{p(x \mid \boldsymbol{D}) \cdot q(x'|x)}. \end{aligned}$$

One common option is the Metropolis choice to choose an acceptance that satisfies detailed balance

$$\mathcal{A}(x'|x) = \min\left(1, \frac{p(x' \mid D)}{p(x \mid D)} \cdot \frac{q_{j'}(xx')}{q_j(x'x)}\right),$$

i.e., one accepts x' as the new state with acceptance probability $\mathcal{A}(x'|x)$. In the extreme cases of $\mathcal{A}(x'|x) = 1$ and $\mathcal{A}(x'|x) = 0$, it is always accepted or rejected, respectively. Since RJMCMC demands for reversible jumps, we will have for every transition from x to x' with proposal probability $q_j(x'|x)$ a reverse transition from x' to x with proposal probability $q'_j(x|x')$.

2.5.3.3. Simulated annealing. To direct the RJMCMC sampling toward an optimum, we combine RJMCMC with Simulated Annealing (Kirkpatrick et al., 1983) which introduces a sequence of decreasing temperatures t_i. With decreasing temperature, less and less jump proposals get accepted. Simulated annealing is integrated in RJMCMC by replacing in the acceptance step both occurrences of $\pi(\cdot)$ in the fraction with $\pi(\cdot)^{1/t_i}$. Theoretically, simulated annealing ensures convergence to the global optimum for any initial configuration using a logarithmic temperature decrease. In our experiments, we used geometric annealing where the new temperature t_{i+1} is calculated by multiplying the current temperature t_i with a constant annealing factor $c_s \in (0,1)$: $t_{i+1} = c_s \cdot t_i$. The start temperature t_0 was set to 1.0 and the annealing factor c_s was set

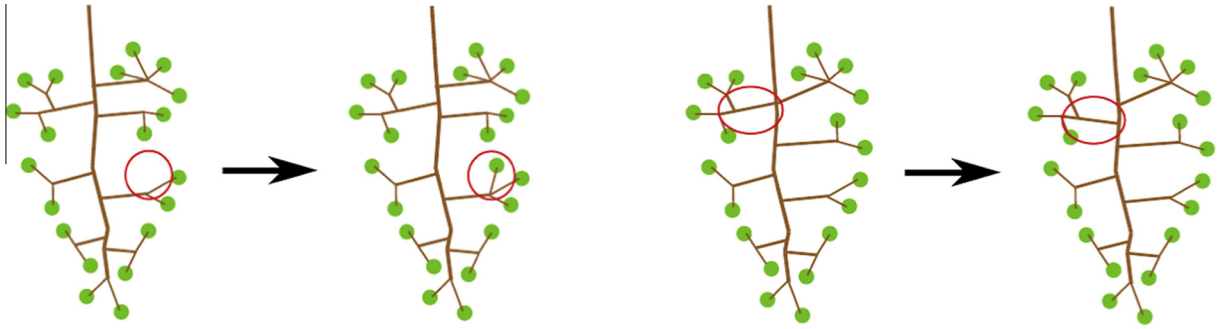

Fig. 8. Illustration of two jump types. Left: jump type *Insert new berry* that will have another jump type *Remove berry* as its reverse jump type. Right: jump type *Move start position of branch-twig* that has itself as reverse jump type.

to 0.99 yielding about 7000–9000 iterations per grape cluster reconstruction.

2.5.3.4. Priors and likelihood. The posterior probabilities used in the acceptance step of RJMCMC provide the opportunity to define the data-driven and model-driven constraints of the optimization problem. In general, the posterior probability can be formulated as the product of two terms $p(x|\boldsymbol{D}) \propto p(x) \cdot \mathcal{L}(\boldsymbol{D}|x)$ by using Bayes' formula.

The likelihood $\mathcal{L}(\boldsymbol{D}|x)$ represents the constraints enforced by the sensor data $\boldsymbol{D}$ in terms of the probability of observing sensor data $\boldsymbol{D}$, given reconstruction hypothesis x. In the development stages BBCH81 and BBCH89 of beginning and full ripeness, we encounter significant occlusions. Thus, the points of the input point cloud have been interpreted completely in terms of the observable components, i.e., the exterior berries and the peduncle. Therefore, we fix these components after the first reconstruction step and interpret them as "pre-processed sensor data". Thereby, we enforce data fitting by connecting the overall architecture of the grape cluster's reconstruction to these exterior components according to the rules of the generative model. In consequence, we can set the likelihood term equal to one in the iterative sampling process. For development stage BBCH73, where almost all components can be sensed by the laser scanner, the likelihood $\mathcal{L}(\boldsymbol{D}|x)$ can be expressed using the sum over all distances between the reconstructed components of hypothesis and the points of the point cloud.

The prior distribution $p(x)$ represents the constraints by the generative model, i.e., the prior distribution $p(x)$ favors reconstruction hypotheses x that are compatible with the generative model. But the space of reconstruction hypotheses shows hypotheses with different numbers of components. Therefore, the prior $p(x)$ must be rewritten as the product of two subcomponents $p(k) \cdot p(\theta_k|k)$ yielding the following formulation of the posterior probability

$$\mathcal{P}(k, \theta_k|\boldsymbol{D}) \propto \mathcal{L}(\boldsymbol{D}|k, \theta_k) \cdot p(k|\theta_k) \cdot p(k).$$

The *model prior* $p(k)$ specifies the probability of the currently chosen hypothesis characteristic, i.e., the number and arrangement of plant components. In our implementation, it is calculated as the product of several prior-subcomponents for the numbers of the different plant components. Every subcomponent of the model prior evaluates for one class of components (branch-twigs, sub-twigs, pedicels, etc.) how probable the actual number of components of this class in a hypothesis is with respect to the value distribution of this component class that was learned in the learning step (cf. Section 2.4.2) of our reconstruction approach based on the training data set. We employed seven prior-subcomponents with their value distributions learned in the learning step: the number of berries (equal to the number of pedicels), the number of nodes on the rachis, the number of twigs branching from the rachis, the number of branch-twigs, the number of sub-twigs, the number of terminal pedicel twigs, and the number of pedicel origins.

The parameter prior $p(\theta_k \mid k)$ models the probability of the currently chosen parameters for the currently chosen hypothesis. In our implementation, it is also calculated as the product of seven prior-subcomponents with their value distributions learned in the learning step (cf. Section 2.4.2): the angles of *twigs* (all twig types), the lengths of *branch-twigs*, the lengths of *sub- twigs*, the lengths of *terminal pedicel twigs*, the lengths of *pedicels*, the angles of *pedicels*, and the sizes of *berry groups*.

2.5.4. Step 4: Derivation of phenotypic descriptors

Given the final and complete reconstruction of a grape cluster the derivation of phenotypic descriptors of the grape cluster can be done in a precise, objective, and reproducible way. The phenotypic descriptors can be derived by taking arbitrary components of a reconstructed grape cluster and all attributes and relations of these components into account.

That way well-known descriptors (e.g. from the OIV list of descriptors) can be derived. Some of these descriptors like the length and width of grape clusters (OIV descriptors 202 and 203, respectively) are well defined and the benefit of applying our approach is just the automation of these measurements.

Some other descriptors are defined originally by means of visual categorizations that might entail problems of rating with respect to subjectivity and comparability. For example, the OIV descriptor 204 categorizes grape clusters with respect to their density into five classes, named as categories 1 ("*very loose*"), 3 ("*loose*"), 5 ("*medium*"), 7 ("*dense*"), and 9 ("*very dense*"). The instructions how to derive OIV descriptor 204 of grape cluster's density is given as follows. "*Examination of the largest bunches of 10 shoots. 1 = berries clearly separated, many visible pedicels; 3berries in loose contact with each other with some visible pedicels; 5 = densely distributed berries, pedicels not visible, berries are movable; 7berries not readily movable; 9 = berries deformed by compression.*" Here, the benefit of applying our approach might not only be the automation of this classification but also the opportunity to derive the categorization in a precise, objective, and reproducible way by employing an appropriate formula. An additional benefit of such automation might also be the potential to define more categories of grape cluster density, i.e., an arbitrary number of degrees of grape cluster's density. In our experiments, we propose the following formula for deriving the density of grape clusters:

$$\frac{\sum_{i=1}^{n} vol(berry_i)}{100 * (\sum_{i=1}^{m} len(twig_i) + len(rachis))},$$

i.e., the sum of volumes of all berries divided by the sum of lengths of all twigs and the rachis. The density grows with more berry volume. But it decreases with longer twigs as the berries get more separated. Hence, the density grows with a higher berry volume and decreases with longer twigs and rachis.

Finally, our approach facilitates the design of novel descriptors in research and their experimental evaluation to derive new valuable descriptors for grapevine breeding.

3. Results

3.1. Reconstruction results

For a quantitative evaluation of our approach, we investigated results on four fully ripe Riesling grape clusters. These clusters are named according to the number of the grapevine in the field and an identifier of the grape cluster on that plant. Here, we use clusters named 51_B, 52_A, 52_B, and 56_B. Moreover, we manually created ground truth data of the stem systems of all four grape clusters. Due to the probabilistic nature of the overall reconstruction process, we computed 100 results for each grape cluster and show distributions of the according values.

Fig. 9 illustrates qualitatively row by row for each of the evaluated grape clusters (1) the point cloud derived by laser scanning, (2) one of the final and complete reconstruction result with berries, and (3) the reconstructed stem architecture of the final reconstruction by removing the berries. The rachis is central, the outer form is well adapted by the twig lengths, and the berry group sizes are reasonable. The point clouds show about 250,000 points in average. The amount of occlusion ranges from around 47% to 64% (volume of occluded interior branching system/volume of grape cluster).

For a quantitative analysis, we evaluated the numbers, lengths, and distances of reconstructed components. This evaluation was performed on 100 reconstruction runs applied to the sensor data of each of the four grape clusters 51_B, 52_A, 52_B, and 56_B.

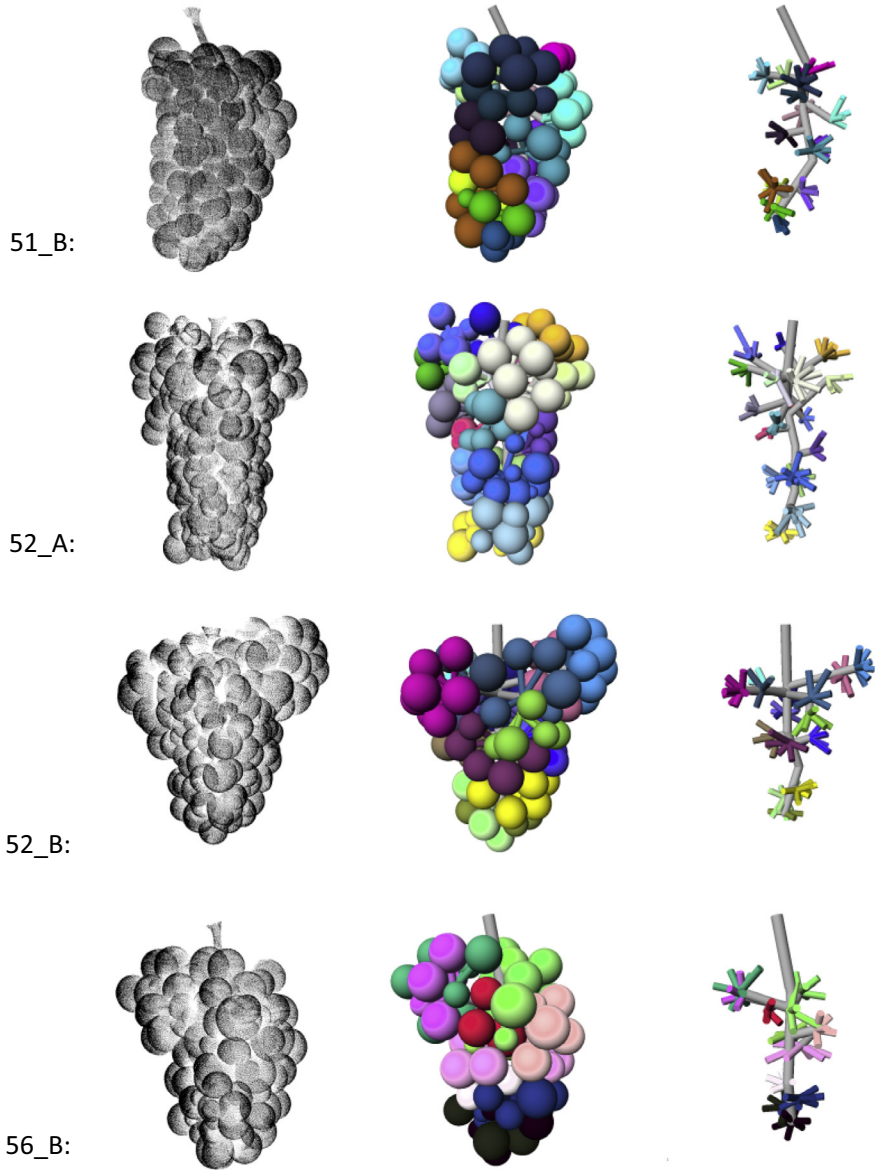

Fig. 9. Experimental results of the reconstruction approach on four fully ripe Riesling grape clusters. Left: The input point cloud generated by laser scanning. Middle: The final complete reconstruction result with berries. Right: the branching architecture of the final result.

Table 1 summarizes the evaluation with respect to the numbers of reconstructed components by comparing the respective quantities of automatically reconstructed components with the corresponding reference values of components derived from the manual reconstructions.

Table 2 summarizes the evaluation with respect to the positions of reconstructed components by comparing positions of the automatically reconstructed components with the positions of components measured in the reference data set. For this part of the evaluation, we established correspondences between the positions of components in the reference data and the positions of components in the automatically generated reconstructions by employing the Hungarian method (Munkres, 1957; Kuhn, 1956, 1955). As input to the Hungarian method, we used for each component type the Euclidean distances between any two components and computed the assignment with the minimal overall distance, i.e., minimal sum of positioning errors.

Table 3 summarizes the evaluation part on comparing for different component types the *sum of lengths* of all reconstructed instances of the respective component type with the corresponding sum of lengths given in the reference data. For a comparison we include the absolute reference values, i.e., the sum of lengths of the respective component type in the reference stem system.

3.2. Phenotyping

Fig. 10 depicts the results for one of the most important phenotypic traits for grapevine in our project, i.e., the density of grape clusters, as a representative example. The grape cluster density is derived by using the formula given in Section 2.5.4, i.e., the sum of volumes of all berries divided by the sum of lengths of all twigs and the rachis. Therefore, the unit of the density is [mm^3/mm].

3.3. Development stages BBCH73 and BBCH81

We also applied our approach to grape clusters of the other two development stages of Riesling and present here one qualitative reconstruction result for each.

Table 1
Estimated *numbers of components* compared to the reference values derived from ground truth data. The values are derived over the four grape clusters 51_B, 52_A, 52_B, and 56_B where every grape cluster was evaluated for 100 reconstruction runs applied to its sensor data.

Component type	Reference number	Mean of estimated number	Standard deviation of estimated number
Grape cluster 51_B			
Rachis nodes	13	9.47	1.08
Branch-twigs	3	2.52	0.54
Sub-twigs	6	2.77	0.66
Terminal pedicel twigs	12	8.51	0.95
Berry groups	22	14.80	0.91
Berries	105	92.50	10.02
Grape cluster 52_A			
Rachis nodes	11	10.79	0.97
Branch-twigs	3	4.13	0.58
Sub-twigs	8	4.51	0.69
Terminal pedicel twigs	10	10.19	1.12
Berry groups	23	19.83	0.40
Berries	123	142.84	13.55
Grape cluster 52_B			
Rachis nodes	7	7.53	1.18
Branch-twigs	4	3.06	0.56
Sub-twigs	6	3.29	0.65
Terminal pedicel twigs	6	7.45	1.17
Berry groups	17	14.80	1.06
Berries	96	110.57	11.66
Grape cluster 56_B			
Rachis nodes	14	7.00	0.97
Branch-twigs	3	2.18	0.38
Sub-twigs	6	2.31	0.50
Terminal pedicel twigs	10	6.21	0.86
Berry groups	20	11.70	0.64
Berries	83	77.85	4.57

Table 2
Overall positioning errors per component type estimated as the *sum of distances* between positions of corresponding components in reference data and automatically generated reconstructions. The values are derived for the four grape clusters 51_B, 52_A, 52_B, and 56_B where every grape cluster was evaluated over 100 reconstruction runs applied to its sensor data.

Component type/grape cluster	Dimensions of grape cluster: length (cm) × width (cm)	Mean of overall positioning error (cm)	Stand. deviation of overall positioning error (cm)
Grape cluster 51_B	10.49 × 5.94		
Rachis nodes		1.0386	0.1994
Branch-twig nodes		0.8476	0.0438
Pedicel origins		0.6262	0.0542
Berries		0.8672	0.0501
Grape cluster 52_A	12.94 × 8.31		
Rachis nodes		0.4006	0.0331
Branch-twig nodes		0.8201	0.0939
Pedicel origins		0.8006	0.0132
Berries		0.8373	0.1199
Grape cluster 52_B	10.88 × 7.74		
Rachis nodes		0.6371	0.0883
Branch-twig nodes		0.7564	0.0212
Pedicel origins		0.7796	0.0763
Berries		0.7660	0.0271
Grape cluster 56_B	9.56 × 5.79		
Rachis nodes		0.8010	0.1065
Branch-twig nodes		0.7946	0.0159
Pedicel origins		0.5094	0.0598
Berries		0.8508	0.0080

Table 3
Overall length errors estimated as *differences between sums of component lengths* of reference data and automatically derived reconstructions, respectively. The values are derived for the four grape clusters 51_B, 52_A, 52_B, and 56_B where every grape cluster was evaluated over 100 reconstruction runs applied to its sensor data.

Component type	Reference sum of lengths (cm)	Mean of overall length error (cm)	Standard deviation of overall length error (cm)
Grape cluster 51_B			
Branch-twigs	4.20	0.2065	1.1918
Sub-twigs	1.95	−0.6093	0.7301
Terminal pedicel twigs	5.75	0.6707	1.1490
Pedicels	92.55	−6.1820	11.1247
Grape cluster 52_A			
Branch-twigs	6.60	1.7320	1.3053
Sub-twigs	2.60	1.1629	0.5982
Terminal pedicel twigs	6.70	4.9509	1.9781
Pedicels	119.95	62.2428	42.0734
Grape cluster 52_B			
Branch-twigs	7.25	−0.6103	1.0910
Sub-twigs	1.90	−0.3336	0.7648
Terminal pedicel twigs	3.30	4.1801	1.8862
Pedicels	106.0	27.1801	30.6428
Grape cluster 56_B			
Branch-twigs	2.65	0.5245	0.5552
Sub-twigs	1.30	−0.5238	0.3244
Terminal pedicel twigs	2.85	0.8758	0.7569
Pedicels	61.25	8.8431	4.0117

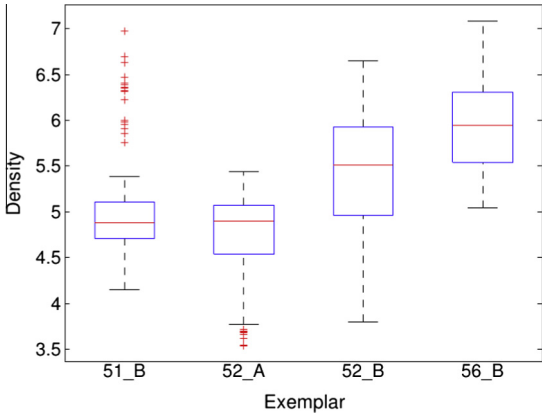

Fig. 10. Results of the automated derivation of the densities of the four grape clusters 51_B, 52_A, 52_B, and 56_B. For each grape cluster, we performed 100 reconstruction runs and determined the density for each of them.

3.3.1. BBCH81: Beginning of ripening

In this development stage, the berries are of almost the same size as in the state of full ripeness. Therefore, the interior is also significantly occluded. Fig. 11 shows an example input point cloud and the according reconstruction result with and without the berries.

3.3.2. BBCH73: Groat-sized berries

In this development stage, the berries are much smaller than in full ripeness, which allows the sensor to capture almost the complete interior of the stem system. Fig. 12 depicts a qualitative example.

3.4. Evaluation of experimental results

Our experimental results show qualitatively that our reconstruction framework of employing an explicit rule-based plant model to control a trans-dimensional probabilistic sampling

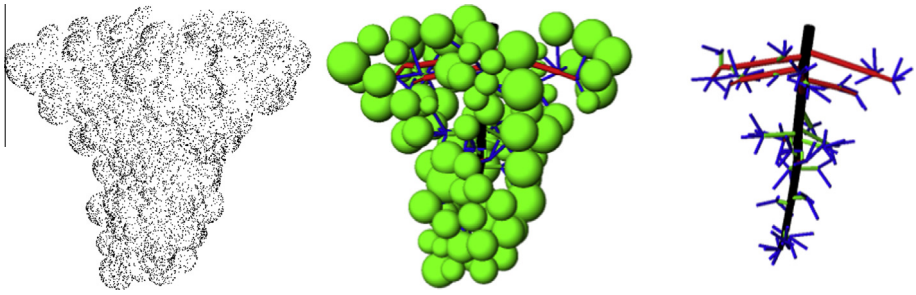

Fig. 11. Example reconstruction result of the development stage beginning of ripening. Left: Input point cloud. Middle: Reconstructed architecture with berries. Right: Reconstructed architecture without berries.

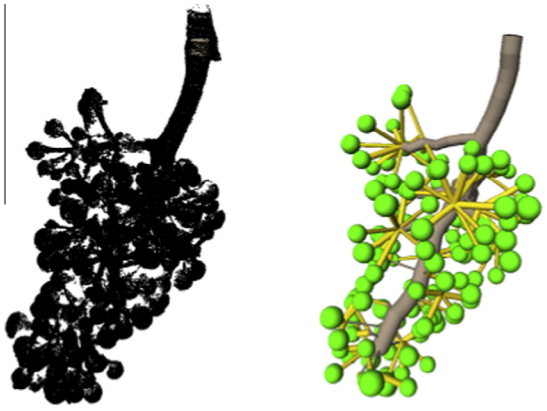

Fig. 12. Example result of a reconstruction given a point cloud of a grape cluster with groat-sized berries.

algorithm is a promising avenue. However, our quantitative results show that we still have not reached the end of this road. Therefore, we discuss here the current state and future work of our reconstruction procedure with respect to the experimental results.

With respect to the number of reconstructed components, we have estimation errors (|mean of estimated numbers – true numbers|) averaged over the four grape cluster experiments of 2.82 for the number of rachis nodes, 0.84 for the number of branch-twigs, 3.28 for the number of sub-twigs, 2.23 for the number of terminal pedicel twigs, 5.22 for the number of berry groups, and 13.02 for the number of berries. Since the berries are together with the peduncle often the only observable anchor features of our complete reconstruction procedure the relatively high averages mean estimation error and the averaged high variance (10.0 compared to values around 1.0 for the other components) of their detection rate suggests improving the reconstruction of the berries in future work. As given in more detail in Section 4.1, our RANSAC-based approach to berry detection itself was shown to be robust with respect to noise and accuracy. However, volume and weight of each berry itself will change position and shape of other berries by pushing and collisions between berries when growing. Therefore, we will use in future work more accurate physical models of the berries that include deformations of the berry surface to have a more realistic model of the surface $\mathcal{S}(b_i)$ of a berry b_i as a result of environmental interactions instead of using spheres. Additionally, we will also include the reconstructed exterior berries of the initial hypothesis into the iterative optimization process to adjust their parameters of position and shape iteratively with respect to the sensor data, i.e., the points of the point cloud. This will yield an explicit likelihood term $\mathcal{L}(\boldsymbol{D}|\boldsymbol{x}) \propto exp\ \left(-\sum_{b_i \in B} \|\mathcal{N}(b_i) - \mathcal{S}(b_i)\|^2\right)$ that corresponds to the sum of the Euclidian distances between the points of the point cloud in a neighborhood $\mathcal{N}(b_i)$ of berry b_i to the surface $\mathcal{S}(b_i)$ of berry b_i in a given reconstruction hypothesis. Finally, we will enhance the information content of the 3D points of a point cloud by using optical sensors to provide depth and color information (cf. Section 4.1) and by deriving local features like orientation and curvature that are characteristic with respect to the types of components (twigs, pedicels, berries, etc.) (Paulus et al., 2013; Behley et al., 2012).

With respect to the position accuracy, a normalization by the averaged reference numbers of Table 1 (where the reference number of sub-twigs is equal to the reference number of branch-twig nodes in Table 2) results in averaged positioning errors of approximately 3 mm for the branch-twig nodes and of less than 1 mm for rachis nodes, pedicel origins, and berries. Compared to the grape clusters' sizes, the positioning errors are about two orders of magnitude smaller. But future work could improve these results further. First, the improved berry reconstruction should also yield higher location accuracy for berries and for the interior components. Second, the jump type that inserts new interior berries can be improved by optimizing first the diameter of a new berry before optimizing its location.

With respect to the determination of the components' lengths, normalization by the averaged reference numbers of Table 1 (where the reference number of berries is equal to the reference number of pedicels in Table 3) shows length errors of about 2–3 mm per component in average. Compared to the grape clusters' sizes, the length errors are again about two orders of magnitude smaller. However, we plan to improve these results. First, the improved berry reconstruction should again yield also a higher accuracy in the length estimation of the twigs. Second, a more flexible jump type for geometrical modifications of the rachis can also improve length estimations.

With respect to phenotyping, the presented example of the formalized variant of the OIV descriptor 204 of grape cluster density shows that the derived median values are in a small range between 5.8 and 6.1 and the boxes containing 50% of all values are in a range between 4.5 and 6.4. Similar results were obtained for other phenotypic descriptors. But of course, these results must be aligned in a representative way with phenotyping results that are derived in the conventional way. This will be part of an upcoming follow-up project.

This up-coming project will also include a representative and accurate analysis of our approach applied to the development stage BBCH73 with groat-sized berries while the results here show only by some first qualitative examples that our approach has the potential to work also on other development stages of grape clusters like BBCH73 and BBCH81 and is therefore promising for monitoring and phenotyping over complete growth periods.

4. Discussion

Our approach to automated 3D reconstruction and phenotyping of grape clusters is based on several assumptions that are discussed here with respect to different aspects of generalization of our approach and with respect to future work.

4.1. Sensors and noise

In our project setting, we used sensor data generated with a *Perceptron ScanWorks V5* laser scanner (Perceptron Inc., 2015) mounted on a *Romer Infinite 2.0* articulated arm (Hexagon Metrology, 2015) producing 3D point clouds with high accuracy of 0.024 mm and high spatial resolution of 0.0137 mm. This raises the question of what will happen (1) if a lower cost sensor with lower precision is used, and (2) if the measurements are noisy. For computational reasons, we first sub-sampled the original 3D point cloud uniformly resulting in approximately 250,000 points per grape cluster. This corresponds to an average point-to-point resolution of 0.19 mm, but nevertheless the high position accuracy of 0.024 mm. Since our reconstruction procedure starts with the detection and reconstruction of the observable exterior components, the robustness of our complete procedure heavily relies on the robustness of the detection of these components. The peduncle is geometrically approximated as a frustum. Frusta are also used to model the geometries of the twigs, the rachis, and the pedicels. For the Riesling cultivar, the berries are geometrically modeled as spheres, for other cultivars other simple geometric approximations like ellipsoids might be used. For the detection of these components, especially the berries, we employ a RANSAC-based method proposed by Schnabel et al. (2007). They evaluated the robustness of their method with respect to position and radius determination experimentally by introducing synthetic position inaccuracy and noise. Applying their evaluation results to our concern of detection and reconstruction of grape clusters' components with the smallest diameters of the smallest pedicels with 1–2 mm and largest diameters of fully ripe berries up to 15 mm, a sensor accuracy of 0.4 mm results in deviations of positioning and size determination of 0.04 mm and 0.05 mm, respectively – even up to a signal-to-noise ratio of 2. This accuracy can be achieved with a semi-professional optical sensor like *Artec EVA* (accuracy up to 0.1 mm, spatial resolution up to 0.5 mm) and *Artec Spider* (accuracy up to 0.05 mm, spatial resolution up to 0.1 mm) (RSI 3D-Systems, 2015). Both sensors are relatively small and lightweight, making them portable and moveable around the object to be measured. Low-cost motion-sensing devices like the *Kinect* are reported to be accurate to within 1–2 mm for distances from 50 cm to 100 cm in most situations (Shin et al., 2013). Also the new *Kinect 2.0* should show accuracy close to 1 mm. Therefore, the current state of low-cost sensors seems not appropriate to deliver sufficiently accurate measurements. In future work, we would like to explore the usage of such a semi-professional optical sensor, because its handling is superior to that of the laser sensor. Additionally, the optical sensor provides intensity and color information that will improve the detection and reconstruction process. For example, the combination of color and depth information is of special interest for the reconstruction of grape clusters of development stage BBCH73, where the diameters of the berries are similar to the diameters of the twigs and therefore more difficult to detect within point clouds without color information.

4.2. Completeness of sensor data

Currently, we are using complete 360° scans of the grape clusters exterior. Therefore, incompleteness of the sensor data is only given due to occlusions of the interior components of a grape cluster caused by its exterior components. In practice, there might be applications where complete 360° scans are not possible or too costly, for example, when aiming to collect sensor data by mobile farm vehicles driving along the vineyard rows. Therefore, future work will include investigations of automated phenotyping based on partial reconstructions of grape clusters.

4.3. Other cultivars and other plants

Our current implementation is tailored to the automated reconstruction and phenotyping of grape clusters. Our experimental evaluation was done with the Riesling cultivar and only with single-winged grape clusters, i.e., grape clusters showing exactly one rachis. Generalization to other grapevine cultivars and double-winged grape clusters are possible, but demand for some feasible adaptations of the berry detector and the generative model's rule set. First, the berry detector has to be generalized to cope with the shape types of grape berries that are listed in the OIV descriptor 223 and can be modeled with simple geometric approximations (i.e., small numbers of shape parameters): globose (spherical), obloid, ovoid, cylindrical, ellipsoid, horn shaped, etc. Second, the rules of the generative modeler must be enriched with rules to model double winged grape clusters.

The generalization to other plant organs and plants will definitely demand for more or less severe adaptations. For example, if leaves need to be modeled explicitly as plant components, they demand for sophisticated modeling approaches. A generative model of leaves must be parsimonious with respect to the number of parameters, but as accurate as possible for the purpose of automated 3D reconstruction and phenotyping. Recently, Henke et al. (2014) presented a model of leaf shapes with polynomials determined by a minimal set of 5–13 real-valued parameters. Additionally, advanced processing algorithms are needed with more complex shaped plant organs and a growing number of parameters. For example, one might use instead of the standard RANSAC approach, improved RANSAC algorithms like R-RANSAC and *Preemptive* RANSAC. An overview on the performance of different RANSAC variants is given by Choi et al. (2009).

In general, we can say that the more complex the plant components with respect to shape, appearance and interactions will be, the more sophisticated the design and the implementation of modeling and reconstruction of the plant must be to keep the balance between computational complexity and robustness of reconstruction.

4.4. Scale space and functional modeling

The generalization from 3D structural modeling to an overall modeling that includes functional modeling in terms of environmental interaction, nutrition flow, photosynthesis, etc. is one strength of the relational growth grammar approach that we have chosen for our generative modeling (Smoleňová et al., 2012). In future work, we intend to include functional aspects to model competition for sunlight and space and the flow of photosynthates.

Multi-scale modeling is known as one of the current challenges in the research field of functional–structural plant modeling (FSPM) (Hanan, 2013) and aims for the integration of structures and dynamics at different spatial and temporal scales. There are various reasons for adopting such an approach. From the theoretical perspective, there is the existence of scientific data at multiple scales. From the practical perspective, there are different scales of screening and monitoring, for example for the purpose of disease and yield estimation. An up-to-date overview and current results in using growth grammars for multi-scale modeling is given by Ong et al. (2014). We are considering this approach to multi-scale

modeling with growth grammars at least with the two scales of single plants and populations in our future work.

4.5. On evaluation

Our current experimental evaluation relies only on 100 reconstruction runs applied to four grape clusters and compares the reconstruction results with ground truth data only in terms of numbers, lengths, and positions of components of the grape clusters. We plan to address this limitation of our current experimental analysis by investigating more grape clusters, i.e., about hundreds of grape clusters, and will evaluate results more explicitly with respect to geometry and structure. For this more comprehensive evaluation, we currently implement and adapt an approach to compare complete branching structures based on a similarity measure between their graph-based representations presented by Boudon et al. (2014).

5. Conclusion

Automated 3D reconstruction is of high importance for efficient plant phenotyping in general. Within a project on grapevine phenotyping, we demonstrated that this can be realized based on the analysis of grape cluster architecture. We developed and implemented a complete processing chain that uses 3D point clouds of grape clusters generated by a laser range sensor and that employs an explicit rule-based generative model of grape cluster architecture. Based on the sensor data and the presented generative model, the processing chain consists of four steps: first, the reconstruction of all visible components of a grape cluster; second, the generation of a first initial 3D reconstruction hypothesis of the complete grape cluster; third, the iterative optimization of the initial 3D reconstruction hypothesis to derive an optimal fitting to the given sensor data thereby complying with the constraints given by the generative model; fourth, the automated derivation of phenotypic descriptors of grape clusters. Due to the usage of the knowledge encoded in the generative model, we are able to derive complete reconstructions even in cases of severe occlusions. Our approach can be used for monitoring and yield estimation in vineyards. The strength of our approach lies in its flexibility in deriving well known phenotypic descriptors as well as the prospects to design new approaches for phenotypic description. Therefore, our approach is suited for grapevine breeding and research on grapevine breeding. First promising experimental results show that our approach could become a new high-throughput and high-resolution phenotyping tool for grapevine breeding. Future work will include different aspects of generalization. First, our approach suggests a paradigm of a model-based processing chain for the automated 3D reconstruction and the automated phenotyping that is capable to deal with occlusions in the sensor data acquisition and is able to extract phenotypic traits in an objective and repeatable way. This paradigm is worth to be investigated with respect to applications on other plant organs, whole plants, and other different plants. Second, our approach will be investigated with respect to other classes of sensor data. Especially, we plan to employ optical sensors and combinations of different sensor modes by fusion of sensor data. Third, future work also includes coherent applications on different scales, e.g., scales of plant organs, whole plants, populations, field, etc. in terms of a multi-scale approach to 3D reconstruction for phenotyping and field monitoring.

Acknowledgements

We thank the German Federal Ministry of Education and Research (funding code: 0315529) and the European Union Funds for regional development (funding code: z1011bc001a) for funding. Furthermore we thank our partners in CROP.SENSe.net for discussions and common work. Especially we thank the working group of Prof. Dr. R. Töpfer from the Julius-Kühn-Institute for Grapevine Breeding in Siebeldingen for selecting and providing the plants, and the working group of Prof. Dr. H. Kuhlmann from the Institute of Geodesy and Geoinformation of Bonn University for generating the sensor measurements.

References

Balfer, J., Schöler, F., Steinhage, V., 2013. Semantic skeletonization for structural plant analysis. Intern. Conf. Funct.–Struct. Plant Model, 42–44.
Behley, J., Steinhage, V., Cremers, A.B., 2012. Performance of histogram descriptors for the classification of 3D laser range data in urban environments. IEEE Int. Conf. Robot. Auto. (ICRA), 4391–4398.
Berenstein, R., Shahar, O.B., Shapiro, A., 2010. Grape clusters and foliage detection algorithms for autonomous selective vineyard sprayer. Intel. Serv. Robot. 3 (4), 233–243.
Binney, J., Sukhatme, G.S., 2009. 3D tree reconstruction from laser range data. IEEE Int. Conf. Robot. Auto., 1321–1326
Boudon, F., Preuksakarn, C., Ferraro, P., Diener, J., Nacry, P., Nikinmaa, E., Godin, C., 2014. Quantitative assessment of automatic reconstructions of branching systems. Ann. Bot. 114 (4), 853–862.
Braun, T., Koch, H., Strub, O., Zolynski, G., Berns, K., 2010. Improving pesticide spray application in vineyards by automated analysis of the foliage distribution pattern in the leaf wall. In: 1st Commercial Vehicle Technology Symposium, pp. 539–548.
Buck-Sorlin, G., Hemmerling, R., Kniemeyer, O., Burema, B., Kurth, W., 2008. A rule-based model of barley morphogenesis, with special respect to shading and gibberellic acid signal transduction. Ann. Bot. 101 (8), 1109–1123.
Choi, S., Kim, T., Yu, W., 2009. Performance evaluation of RANSAC family. British Machine Vision Conference (BMVC), pp. 81.1–81.12.
Côté, J.-F., Widlowski, J.-L., Fournier, R.A., Verstraete, M.M., 2009. The structural and radiative consistency of three-dimensional tree reconstructions from terrestrial lidar. Remote Sens. Environ. 113 (5), 1067–1081.
CROP.SENSe.net, 2015. CROP.SENSe.net Competence network for phenoyping research. <http://www.cropsense.uni-bonn.de/> (accessed 27.03.15).
Cubero, S., Diago, M.P., Blasco, J., Tardáguila, J., Prats-Montalbán, J.M., Ibáñez, J., Tello, J., Aleixos, N., 2015. A new method for assessment of bunch compactness using automated image analysis. Aust. J. Grape Wine Res. 2, 101–110.
Delenne, C., Durrieu, S., Rabatel, G., Deshayes, M., 2010. From pixel to vine parcel: a complete methodology for vineyard delineation and characterization using remote-sensing data. Comput. Electron. Agric. 70 (1), 78–83.
Diago, M.P., Correa, C., Millan, B., Barreiro, P., Valero, C., Tardaguila, J., 2012. Grapevine yield and leaf area estimation using supervised classification methodology on RGB images taken under field conditions. Sensors 12 (12), 16988–17006.
Diago, M.P., Sanz-Garcia, A., Millan, B., Blasco, J., Tardaguila, J., 2014. Assessment of flower number per inflorescence in grapevine by image analysis under field conditions. J. Sci. Food Agric. 94 (10), 1981–1987.
Dornbusch, T., Wernecke, P., Diepenbrock, W., 2007. A method to extract morphological traits of plant organs from 3D point clouds as a database for an architectural plant model. Ecol. Model. 200, 119–129.
Font, D., Pallejà, T., Tresanchez, M., Runcan, D., Moreno, J., Martinez, D., Teixidó, M., Palacín, J., 2014a. A proposal for automatic fruit harvesting by combining a low cost stereovision camera and a robotic arm. Sensors 14, 11557–11579.
Font, D., Pallejà, T., Tresanchez, M., Teixidó, M., Martinez, D., Moreno, J., Palacín, J., 2014b. Counting red grapes in vineyards by detecting specular spherical reflection peaks in RGB images obtained at night with artificial illumination. Comput. Electron. Agric. 108, 105–111.
Frasson, R.P.d.M., Krajewski, W.F., 2007. Three-dimensional digital model of a maize plant. Agric. For. Meteorol. 150, 478–488.
Fuentes, S., Poblete-Echeveirría, C., Ortega-Farias, S.T.S., De Bei, R., 2014. Automated estimation of leaf area index from grapevine canopies using cover photography, video and computational analysis methods. Aust. J. Grape Wine Res. 20 (3), 465–473.
Furbank, R.T., Tester, M., 2011. Phenomics – technologies to relieve the phenotyping bottleneck. Trends Plant Sci. 16 (2), 635–644. http://dx.doi.org/10.1016/j.tplants.2011.09.005.
Green, P.J., 1995. Reversible jump markov chain Monte Carlo computation and bayesian model determination. Biometrika 82 (4), 711–732.
Green, P.J., 2003. Trans-dimensional Markov chain Monte Carlo. In: Green, P.J., Hjort, N.L., Richardson, S. (Eds.), Highly Structured Stochastic Systems. Oxford University Press, 179, p. 198.
Hall, A., Louis, J., Lamb, D., 2003. Characterising and mapping vineyard canopy using high-spatial-resolution aerial multispectral images. Comput. Geosci. 29 (7), 813–822.
Hanan, J., 2013. Functional–structural modelling with L-systems: where from and where to. Proc. 7th Intern. Conf. on Functional–Structural Plant Models, pp. 1–3.
Hartmann, A., Czauderna, T., Hoffmann, R., Stein, N., Schreiber, F., 2011. Htpheno: an image analysis pipeline for high-throughput plant phenotyping. BMC Bioinf. 12, 148–156.

Hemmerling, R., Evers, J.B., Smoleňová, K., Buck-Sorlin, G., Kurth, W., 2013. Extension of the GroIMP modelling platform to allow easy specification of differential equations describing biological processes within plant models. Comput. Electron. Agric. 92, 1–8.
Hemmerling, R., Kniemeyer, O., Lanwert, D., Kurth, W., Buck-Sorlin, G., 2008. The rule-based language XL and the modelling environment GroIMP illustrated with simulated tree competition. Funct. Plant Biol. 35, 739–750.
Henke, M., Huckemann, S., Kurth, W., Sloboda, B., 2014. Reconstructing leaf growth based on non-destructive digitizing and low-parametric shape evolution for plant modelling over a growth cycle. Silva Fennica 48 (2), article id. 1019.
Hexagon Metrology, 2015. Hexagon metrology, Inc. <http://www.hexagonmetrology.us/> (accessed 27.03.15).
Huang, C.-Y., Jheng, W.-T., Tai, W.-K., Chang, C.-C., Way, D.-L., 2013. Procedural grape bunch modeling. Comput. Graph. 37 (4), 225–237.
Huang, H., Mayer, H., 2007. Extraction of 3D unfoliaged trees from image sequences via a generative statistical approach. Lect. Notes Comput. Sci. 4713, 385–394.
IPGRI, 2015. International Plant Genetic Resources Institute, Rome, Italy, renamed to Bioversity International. <http://www.bioversityinternational.org/> (accessed 27.03.15).
IPGRI, UPOV, OIV, 1997. Descriptors for Grapevine (Vitis ssp.), International Union for the Protection of New Varieties of Plants, Geneva, Switzerland/Office Internationale de la Vigne et du Vin, Paris, France/International Plant Genetic Resources Institute, Rome, Italy.
Ivorra, E., Sánchez, A.J.S., Camarasa, J.G., Diago, M.P., Tardaguila, J., 2015. Assessment of grape cluster yield components based on 3D descriptors using stereo vision. Food Control 50, 273–282.
JKI, 2015. Julius Kühn Institute for Grapevine Breeding. <http://www.jki.bund.de/de/startseite/institute/zuechtung-reben.html> (accessed 27.03.15).
Johnson, L.F., Roczen, D.E., Youkhana, S.K., Nemani, R.R., Bosch, D.F., 2003. Mapping vineyard leaf area with multispectral satellite imagery. Comput. Electron. Agric. 38 (1), 33–44.
Kicherer, A., Herzog, K., Pflanz, M., Wieland, M., Rüger, P., Kecke, S., Kuhlmann, H., Töpfer, R., 2015. An automated field phenotyping pipeline for application in grapevine research. Sensors 15 (3), 4823–4836.
Kirkpatrick, S., Gelatt, C.D., Vecchi, M.P., 1983. Optimization by simulated annealing. Science 220 (4598), 671–680.
Kniemeyer, O., 2008. Design and Implementation of a Graph Grammar Based language for Functional–Structural Plant Modeling. Ph.D. thesis. Technical University Cottbus.
Kniemeyer, O., Barczik, G., Hemmerling, R., Kurth, W., 2008. Relational growth grammars – a parallel graph transformation approach with applications in biology and architecture. proc. of symposium on applications of graph transformations with industrial relevance AGTIVE 2007, in Lecture Notes in Computer Science, vol. 5008, pp. 152–167.
Kuhn, H.W., 1955. The Hungarian method for the assignment problem. Naval Res. Logist. Q. 2 (1–2), 83–97.
Kuhn, H.W., 1956. Variants of the Hungarian method for assignment problems. Naval Res. Logist. Q. 3 (4), 253–258.
Liu, S., Marden, S., Whitty, M., 2013. Towards automated yield estimation in viticulture. Proc. Aust. Conf. Robot. Autom.
Livny, Y., Yan, F., Olson, M., Chen, B., Zhang, H., El-Sana, J., 2010. Automatic reconstruction of tree skeletal structures from point clouds. ACM Trans. Graph. 29 (6), 151:1–151:8.
Llorens, J., Gil, E., Llop, J., Queraltó, M., 2011. Georeferenced LiDAR 3D vine plantation map generation. Sensors 11, 6237–6256.
Longo, D., Pennissi, A., Bonsignore, R., Muscato, G., Schillaci, G., 2010. A multifunctional tracked vehicle able to operate in vineyards using gps and laser range-finder technology. Intern. Conf. Ragusa SHWA2010, pp. 487–492.
Lorenz, D.H., Eichhorn, K.W., Bleiholder, H., Klose, R., Meier, U., Weber, E., 1995. Growth stages of the grapevine: phenological growth stages of the grapevine (*Vitis vinifera* L. ssp. vinifera) – codes and descriptions according to the extended BBCH scale. Aust. J. Grape Wine Res. 1 (2), 100–103.
MacQueen, J., 1967. Some methods for classification and analysis of multivariate observations. Berkeley Symp. Math. Stat. Probab., 281–297
Mazzetto, F., Calcante, A., Mena, A., Sacco, P., 2011. Test of ground-sensing devices for monitoring canopy vigour and downy mildew presence in vineyards: first qualitative traits. J. Agric. Eng. 42, 1–9.
Möller, M., Alchanatis, V., Cohen, Y., Meron, M., Tsipris, J., Naor, A., Ostrovsky, V., Sprintsin, M., Cohen, S., 2007. Use of thermal and visible imagery for estimating crop water status of irrigated grapevine. J. Exp. Bot. 58, 827–838.
Munkres, J., 1957. Algorithms for the assignment and transportations problems. SIAM J. Appl. Math. 5 (1), 32–38.
Nuske, S., Wilshusen, K., Achar, S., Yoder, L., Narasimhan, S., Singh, S., 2014. Automated visual yield estimation in vineyards. J. Field Robot. 31, 837–860.
OIV, 2009. Descriptor List for Grape Varieties and Vitis Species, second ed. <http://www.oiv.int/oiv/files/5%20-%20Publications/5%20-%201%20Publications%20OIV/EN/5-1-9_Liste_descripteurs_2ed_EN.pdf> (accessed 27.03.15).
OIV, 2015. Organisation Internationale de la Vigne et du Vin, Paris, France. <http://www.oiv.int/> (accessed 27.03.15).
Ong, Y., Streit, K., Henke, M., Kurth, W., 2014. An approach to multiscale modelling with graph grammars. Ann. Bot. 114 (4), 813–827.
Pallas, B., Loi, C., Christophe, A., Cournède, P.-H., Lecoeur, J., 2009. A stochastic growth model of grapevine with full interaction between environment, trophic competition and plant development. Intern. Symp. on Plant Growth Modeling, Simulation, Visualization and Applications, pp. 95–102.
Paproki, A., Sirault, X., Berry, S., Furbank, R.J.F., 2012. A novel mesh processing based technique for 3D plant analysis. BMC Plant Biol. 12, 63.
Paulus, S., Dupuis, J., Mahlein, A.-K., Kuhlmann, H., 2013a. Surface feature based classification of plant organs from 3D laser scanned point clouds for plant phenotyping. BMC Bioinformatics 14, 238.
Paulus, S., Dupuis, J., Mahlein, A.-K., Kuhlmann, H., 2013b. Surface feature based classification of plant organs from 3D laser scanned point clouds for plant phenotyping. BMC Bioinformatics.
Perceptron Inc., 2015. Perceptron Inc. <http://www.perceptron.com> (accessed 27.03.15).
Preuksakarn, C., Boudon, F., Ferraro, P., Durand, J.-B., Nikinmaa, E., Godin, C., 2010. Reconstructing plant architecture from 3D laser scanner data. Proc. 6th Intern. Workshop on Functional–Structural Plant Models, pp. 16–18.
Prusinkiewicz, P., Lindenmayer, A., 1990. The Algorithmic Beauty of Plants. Springer.
Raumonen, P., Kaasalainen, M., Akerblom, M., Kaasalainen, S., Kaartinen, H., Vastaranta, M., Holopainen, M., Disney, M., Lewis, P., 2013. Fast automatic precision models from terestrical laser scanner data. Remote Sensing 5 (2), 491–520.
Roscher, R., Herzog, K., Kicherer, A., Kunkel, A., Töpfer, R., Förstner, W., 2014a. Automated image analysis framework for high-throughput determination of grapevine berry sizes using conditional random fields. Comput. Electron. Agric. 100, 148–158.
Roscher, R., Herzog, K., Kunkel, A., Kicherer, A., Töpfer, R., Förstner, W., 2014b. Automated image analysis framework for high-throughput determination of grapevine berry sizes using conditional random fields. Comput. Electron. Agric., 148–158
RSI 3D-Systems, 2015. RSI 3D-Systems. <http://www.rsi-3dsystems.com/> (accessed 27.03.15).
Runions, A., Lane, B., Prusinkiewicz, P., 2007. Modeling trees with a space colonization algorithm. Proc. Eurographics Workshop on Natural Phenomena 2007, pp. 63–70.
Schnabel, R., Wahl, R., Klein, R., 2007. Efficient RANSAC for point-cloud shape detection. Comput. Graph. Forum 26 (2), 214–226.
Schöler, F., 2014. 3D Reconstruction of Plant Architecture by Grammar-based Modeling and Markov Chain Sampling. PhD Thesis, University of Bonn.
Schöler, F., Balfer, J., Steinhage, V., 2013. Automated parameter estimation for a plant architecture model. Int. Conf. Funct.–Struct. Plant Model, 22–24.
Shin, B., Venkatramani, R., Borker, P., Olch, A., Grimm, J., Wong, K., 2013. Spatial accuracy of a low cost high resolution 3D surface imaging device for medical applications. Int. J. Med. Phys., Clin. Eng. Radiat. Oncol. 2, 45–51.
Shlyakhter, I., Rozenouer, M., Dorsey, J., Teller, S., 2001. Reconstructing 3D tree models from instrumented photographs. IEEE Comput. Graphics Appl. 21 (3), 53–61.
Smith, K.C., 2007. Bayesian Methods for Visual Multi-Object Tracking with Applications to Human Activity Recognition. PhD Thesis, Ecole Polytechnique Fédérale de Lausanne, Lausanne, Switzerland.
Smoleňová, K., Henke, M., Winfried Kurth, W., 2012. Rule-based integration of GreenLab into GroIMP with GUI aided parameter input. IEEE 4th Intern. Symp. on Plant Growth Modeling, Simulation, Visualization and Applications (PMA12), pp. 347–354.
Tello, J., Ibánez, J., 2014. Evaluation of indexes for the quantitative and objective estimation of grapevine bunch compactness. Vitis – J. Grap. Res. 53 (1), 9–16.
UPOV, 2015. Union for the Protection of New Varieties of Plants, Geneva, Switzerland. <http://www.upov.int/> (accessed 27.03.15).
Vail, M.E., Marois, J.J., 1991. Grape cluster architecture and the susceptibility of berries to Botrytis cinerea. Phytopathology 81, 188–191.
Xu, H., Gosset, N., Chen, B., 2007. Knowledge and heuristic-based modeling of laser-scanned trees. ACM Trans. Graph. 26 (4), 19:1–19:13.
Zarco-Tejada, P.J., Berjón, A., López-Lozano, R., Miller, J.R., Martín, P., Cachorro, V., González, M.R., de Frutos, A., 2005. Assessing vineyard condition with hyperspectral indices: leaf and canopy reflectance simulation in a row-structured discontinuous canopy. Remote Sens. Environ. 99 (3), 271–287.